# Coherent potential approximation of random nearly isostatic kagome lattice

Xiaoming Mao and T. C. Lubensky
*Department of Physics and Astronomy, University of Pennsylvania, Philadelphia, Pennsylvania 19104, USA*
(Received 11 August 2010; revised manuscript received 19 October 2010; published 18 January 2011)

The kagome lattice has coordination number 4, and it is mechanically isostatic when nearest-neighbor sites are connected by central-force springs. A lattice of $N$ sites has $O(\sqrt{N})$ zero-frequency floppy modes that convert to finite-frequency anomalous modes when next-nearest-neighbor (NNN) springs are added. We use the coherent potential approximation to study the mode structure and mechanical properties of the kagome lattice in which NNN springs with spring constant $\kappa$ are added with probability $\mathcal{P} = \Delta z/4$, where $\Delta z = z - 4$ and $z$ is the average coordination number. The effective medium static NNN spring constant $\kappa_m$ scales as $\mathcal{P}^2$ for $\mathcal{P} \ll \kappa$ and as $\mathcal{P}$ for $\mathcal{P} \gg \kappa$, yielding a frequency scale $\omega^* \sim \Delta z$ and a length scale $l^* \sim (\Delta z)^{-1}$. To a very good approximation at small nonzero frequency, $\kappa_m(\mathcal{P},\omega)/\kappa_m(\mathcal{P},0)$ is a scaling function of $\omega/\omega^*$. The Ioffe-Regel limit beyond which plane-wave states become ill-defined is reached at a frequency of order $\omega^*$.

DOI: 10.1103/PhysRevE.83.011111 PACS number(s): 46.65.+g, 05.70.Jk, 61.43.−j, 62.20.de

## I. INTRODUCTION

Understanding the nature of mechanical stability, how it arises, and how it can be controlled is important to fields ranging from civil engineering to biology. Materials and systems that undergo a transition from a floppy state that cannot support an external load to a rigid state [1] that can include frames, studied by Maxwell [2], of points connected by fixed length struts, randomly diluted lattices of springs that undergo a rigidity percolation transition [3–5] upon dilution, network glasses [3,6], granular media [7,8], networks of cross-linked semiflexible polymers [9–11], and packed spheres near the jamming transition [12–14]. The transition state separating the floppy from the rigid state is either at or near a special "isostatic" state in which the number of constraints (struts in the case of the Maxwell frames) is such that there are no zero-energy modes, other than the trivial ones arising from rigid translations and rotations, and such that the removal of one constraint leads to the appearance of an extra zero-frequency internal floppy mode. For systems of particles or points in $d$ dimensions in which neighboring sites interact via central-force potentials, the isostatic point occurs when $z$, the average number of neighbors per site is equal to $2d$. The square and kagome lattices in two dimensions and the simple cubic and pyrochlore lattices in three dimensions are systems whose bulk sites have exactly $2d$ nearest-neighbor sites, and apart from corrections arising from boundary sites with only $2d - 1$ or fewer neighbors, they are isostatic. Because they are fully characterized and because they can be moved off isostaticity in precise and well-controlled ways, they are attractive platforms for studying what effects the existence of nearby isostatic point have on elastic response and mode structure [15,16] of elastic networks. In this paper, we use the coherent potential approximation (CPA) [17–20] to study frequency-dependent mechanical response and mode structure of a kagome lattice of nearest-neighbor harmonic springs with spring constant $k$ to which next-nearest-neighbor springs of spring constant $\kappa$ are randomly added with probability $\mathcal{P}$.

### A. The Maxwell argument

Maxwell considered a frame of $N$ points in $d$ dimensions connected by struts of fixed length, though his arguments apply equally well to systems in which the struts are replaced by central-force potentials. Each point in the frame has $dN$ translational degrees of freedom, and in the absence of struts, these points have $dN$ zero modes. Thus, the total number of zero modes is $N_0 = dN - N_c$, where $N_c$ is the number of constraints, provided that $dN - N_c$ is greater than $d(d + 1)/2$, the number of trivial modes of translation and rotation of a rigid body. Since each strut is shared by two sites, there are $zN/2$ struts, where $z$ is the average number of neighbors per site, and if all struts are independent, then $N_0 = dN - \frac{1}{2}zN$. In large systems the trivial modes can be neglected in the total count, and the critical number of neighbors below which there are nontrivial zero modes, called *floppy modes* or *mechanisms* [21,22], is $z_c = 2d$. If $z > z_c$, the system has no floppy modes, and the system is rigid. The counting of floppy modes is different if there are bending as well as stretching forces [3,23,24] and if there are redundant struts [25–27] in the network whose addition does not change $N_0$, but for each realization of the network, there is a critical value of $z$ separating a floppy state with $N_0 > 0$ from a rigid one whose macroscopic elastic moduli are nonzero and that can thus support external loads. Thus, $z = z_c$ is a kind of mechanical critical point.

### B. Examples of rigidity transitions

Rigidity percolation [3,4] is probably the most studied of the transitions to rigidity. It is analogous to the connectivity percolation problem [28,29], but its threshold is different and it is in a different universality class. In its simplest form, nearest-neighbor bonds on a lattice are populated with central-force springs with probability $\mathcal{P}$. At a critical probability, $\mathcal{P} = \mathcal{P}_r$, a rigid cluster forms, and for $\mathcal{P} > \mathcal{P}_r$, all elastic moduli grow continuously from zero. This behavior occurs in randomly diluted random [30,31] as well as periodic lattices. The probability that a site is a member of the infinite rigid cluster also grows continuously from zero [25,32] in $2d$, but in the fcc and bcc bond-diluted lattices in $3d$ [27], it jumps discontinuously to a nonzero value. Thus, in the latter lattices, the central-force rigidity transition is first order in terms of the geometry of the rigid cluster but second order in terms of the elastic moduli. Effective medium theories [33–35]

 

provide a remarkably accurate description of the growth of elastic moduli above $\mathcal{P}_r$ and the zero modes count below $\mathcal{P}_r$ [36]. The addition of bending forces between neighboring bonds [3,24,37] provides an important generalization of central-force models that provide realistic descriptions of network glasses [3,24,26] and of networks of semiflexible polymers [9–11,38,39].

The jamming of packed spheres [12,40] is another example of a rigidity transition. Spheres of radius $a$ are characterized by their volume fraction $\phi$. Below a critical fraction $\phi_c$, spheres are on average not constrained by their neighbors, and above $\phi_c$, there are a sufficient number of contacts between them that the system as a whole supports both compression and shear. At the jamming point $J$ where $\phi = \phi_c$, the average coordination number is $z_c = 2d$, making the state at $J$ isostatic in the Maxwell sense. For $\Delta\phi = (\phi - \phi_c) > 0$, $\Delta z = z - z_c \sim (\Delta\phi)^{1/2}$, and the shear modulus scales as $G \sim (\Delta\phi)^{1/2} \sim \Delta z$ [13,41]. Interestingly, the bulk modulus $B$ is nonzero at $J$, and $B \sim (\Delta\phi)^0 \sim (\Delta z)^0$ [13,41]. Thus, in terms of the bulk modulus, the jamming transition is first order, whereas in terms of the shear modulus, it is second order. Associated with this transition is a divergent characteristic length scale $l^* \sim (\Delta\phi)^{-1/2} \sim (\Delta z)^{-1}$ and a vanishing frequency scale $\omega^* \sim (\Delta\phi)^{1/2} \sim (\Delta z)$ [42–44], whose scaling properties can be derived from a simple cutting argument [45,46]. $\omega^*$ marks the transition in the density of states [45] from a Debye regime to a frequency-independent regime characteristic of a one-dimensional system, and $l^*$ can be interpreted as the length scale at which the longitudinal phonon frequency is equal to $\omega^*$. There is a second length that diverges as $(\Delta z)^{-1/2}$, which appears to be associated with thermal transport [47,48], though it is also the length scale at which the transverse sound frequency is equal to $\omega^*$.

The close-packed spheres at the jamming transition is isostatic with an average of $2d$ neighbors per site. The cutting arguments that determine the dependence of $\omega^*$ and $l^*$ on $\Delta z$ appear to depend only on the existence of a nearby isostatic state and not on the exact nature of that state, suggesting that they might apply quite generally to any system that becomes rigid at an isostatic point. (To our knowledge, they have not been applied to the rigidity percolation transition, which has a threshold slightly below the isostatic limit [5,25,27].) To explore this possibility, it is natural to study the properties of precisely determined periodic isostatic lattices that can be moved away from isostaticity as a complement to the study of random isostatic or nearly isostatic lattices generated by random dilution or by sphere packing. Periodic isostatic lattices, like the square and kagome lattices, can be moved away from isostaticity by adding next-nearest-neighbor (NNN) springs with spring constant $\kappa$ either homogeneously on all NNN bonds or randomly on these bonds with probability $\mathcal{P}$. In the former case, isostaticity is approached continuously as $\kappa \to 0$, and in the latter case, it is approached by either $\mathcal{P} \to 0$ or $\kappa \to 0$ or by both. Exact calculations on the square and kagome lattices [15] with NNN springs uniformly added reveal a characteristic frequency $\omega^* \sim \kappa^{1/2}$ and length $l^* \sim \kappa^{-1/2}$. In the square lattice, the compression modulus $C_{11}$ remains nonzero as $\kappa \to 0$, but the shear modulus $C_{11} \sim \kappa$ vanishes with $\kappa$. In the kagome lattice, both the bulk and the shear modulus remain nonzero in this limit. Within the CPA approximation in the random case [16], the static spring constant $\kappa_m(0)$ is proportional to $\mathcal{P} \sim \Delta z$ for $\mathcal{P} > \kappa/k$ and to $\mathcal{P}^2 \sim (\Delta z)^2$ for $\mathcal{P} < \kappa/k$, indicating a crossover from nearly affine behavior at large $\mathcal{P}$ to nonaffine behavior as $\mathcal{P} \to 0$. This implies that near the isostatic limit, $\omega^* \sim \Delta z$ and $l^* \sim \kappa_m^{-1/2} \sim (\Delta z)^{-1}$, in agreement with the cutting argument. Furthermore, $\kappa_m(\omega) = \kappa_m(0) f(\omega/\omega^*)$, where $f$ is a scaling function. On the other hand, $C_{44} \sim \kappa_m \sim (\Delta z)^2$ vanishes more rapidly than does the shear modulus at jamming.

### C. Review of results

In this paper, we undertake a CPA analysis of the kagome lattice with added NNN springs. As in the case of the square lattice, we find nonaffine response with $\kappa_m(0) \sim \mathcal{P}^2$ at small $\mathcal{P}$ and nearly affine response with $\kappa_m(0) \sim \mathcal{P}$ at large $\mathcal{P}$, and as a result $\omega^* \sim \Delta z$ and $l^* \sim (\Delta z)^{-1}$, again in agreement with the cutting argument. We also find that $\kappa_m(\mathcal{P},\omega)/\kappa_m(\mathcal{P},0)$ is a basically a scaling function of $\omega/\omega^*$ at small $\mathcal{P}$, but with small yet important deviations at small $\omega$ that describe Rayleigh scattering, characterized by a mean-free path that scales as $\omega^{-3}$ in $2d$. Thus, the cutting argument provides a consistent description of the frequency and length scales for systems near three isostatic networks with qualitatively different geometries, with differences reflected in the different behaviors as a function of $\Delta z$ of their elastic moduli and of their different mode structures. It would be tempting to conclude that the cutting argument applies universally to all systems near isostaticity, but that would perhaps be a little premature. There are indications [49] that it does not apply to models, such as one obtained by twisting the unit cells of the kagome lattice, in which the bulk modulus, but not the shear modulus vanishes in the isostatic limit.

The outline of this paper is as follows. In Sec. II we review the elasticity of the homogeneous nearly isostatic kagome lattice. In Sec. III we discuss the CPA on random nearly isostatic kagome lattices with the NNN bonds randomly occupied with probability $\mathcal{P}$. In Sec. IV we discuss the results of the CPA calculation, including the crossover of $\kappa_m$ from $\mathcal{P}^2$ to $\mathcal{P}$ behavior as $\mathcal{P}$ increase or $\kappa$ decreases and the rapid increase of scattering at the characteristic frequency $\omega_D^* \sim \Delta z$.

## II. HOMOGENEOUS NEARLY ISOSTATIC KAGOME LATTICE AND ITS ELASTICITY

### A. Expansion of elastic energy in general lattice models

In this section we briefly review the elastic energy in central-force network models, in which the elastic energy $U$ can be written as a sum of the energy of each central-force bond,

$$U = \sum_b U_b(R_b), \tag{1}$$

where $R_b$ is the length of the bond and $U_b$ is the potential energy of the bond as a function of the length. We consider a displacement field on the network that maps particle $\ell$ which is at position $\mathbf{R}_{\ell 0}$ to a new position $\mathbf{R}_\ell = \mathbf{R}_{\ell 0} + \mathbf{u}_\ell$; thus, the length of bond $b$ between particles $\ell$ and $\ell'$ is changed to

$$R_b = |\mathbf{R}_{\ell'} - \mathbf{R}_\ell|. \tag{2}$$

We refer to the original space in which particle $\ell$ is at $\mathbf{R}_{\ell 0}$ as the *reference space* and the space after applying the displacement field as the *target space*. We consider harmonic potentials,

$$U_b = \frac{k_b}{2}(R_b - R_{bR})^2, \tag{3}$$

where $R_{bR}$ is the rest length of the bond and $k_b$ is the spring constant. The length $R_b$ can be expanded for small displacement $\mathbf{u}$ as

$$R_b = R_{b0} + \mathbf{e}_{b0}\cdot\mathbf{u}_b + \frac{1}{2R_{b0}}\mathbf{u}_b\cdot(\mathbf{I}-\mathbf{e}_{b0}\mathbf{e}_{b0})\cdot\mathbf{u}_b + O\left(\mathbf{u}_b^3\right), \tag{4}$$

where $R_{b0} = |\mathbf{R}_{\ell' 0} - \mathbf{R}_{\ell 0}|$, $\mathbf{u}_b = \mathbf{u}_{\ell'} - \mathbf{u}_\ell$, and $\mathbf{e}_{b0} = (\mathbf{R}_{\ell' 0} - \mathbf{R}_{\ell 0})/|\mathbf{R}_{\ell' 0} - \mathbf{R}_{\ell 0}|$ is the unit vector pointing along the bond in the reference space. Thus, we have

$$U_b = \frac{k_b}{2}(R_{b0} - R_{bR})^2 + f_b\,\mathbf{e}_{b0}\cdot\mathbf{u}_b + \frac{1}{2}\mathbf{u}_b\cdot\left[k_b\mathbf{e}_{b0}\mathbf{e}_{b0} + \frac{f_b}{R_{b0}}(\mathbf{I}-\mathbf{e}_{b0}\mathbf{e}_{b0})\right]\cdot\mathbf{u}_b, \tag{5}$$

where $f_b = U_b'(R) = k_b(R_{b0} - R_{bR})$ is the magnitude of the force on the bond in the reference space. In general, we consider the case in which the reference state is in mechanical equilibrium, which means that the total force on each particle vanishes,

$$\mathbf{f}_\ell = \sum_{b(\ell,\ell')} f_b\mathbf{e}_{b0} = 0, \tag{6}$$

where the sum $\sum_{b(\ell,\ell')}$ is over all occupied bonds connected to $\ell$. However, to capture the properties of random networks, which often carry residual stress, the length of each bond is not necessarily at its rest length; that is, $R_{b0} - R_{bR} \neq 0$ in general.

The change of the elastic energy from the reference space to the target space of the whole system is then a quadratic form of the displacement field,

$$\Delta U = \sum_b \frac{1}{2}\mathbf{u}_b\cdot\left[k_b\mathbf{e}_{b0}\mathbf{e}_{b0} + \frac{f_b}{R_{b0}}(\mathbf{I}-\mathbf{e}_{b0}\mathbf{e}_{b0})\right]\cdot\mathbf{u}_b, \tag{7}$$

which can also been written as

$$\Delta U = \sum_b \frac{1}{2}\left[k_b(\mathbf{u}_b^{\parallel})^2 + \frac{f_b}{R_{b0}}(\mathbf{u}_b^{\perp})^2\right], \tag{8}$$

where $\mathbf{u}_b^{\parallel}$ is the component of $\mathbf{u}_b$ parallel to $\mathbf{e}_{b0}$ and $\mathbf{u}_b^{\perp}$ is the component perpendicular to $\mathbf{e}_{b0}$.

By doing a gradient expansion on the displacement field,

$$\mathbf{u}_b = R_{b0}\,e_{b0k}\,\partial_k\mathbf{u}(\mathbf{r}), \tag{9}$$

where $\mathbf{u}(\mathbf{r})$ is the displacement field at position $\mathbf{r}$, we recover the elastic energy of the continuum theory,

$$\Delta U = \int d\mathbf{r} K_{ijkl}\partial_k u_i\partial_l u_j, \tag{10}$$

with

$$K_{ijkl} = \sum_{\mathbf{b}}\frac{R_{b0}^2}{2v_0}e_{b0k}e_{b0l}\times\left[k_b e_{b0i}e_{b0j} + \frac{f_b}{R_{b0}}(\delta_{ij} - e_{b0i}e_{b0j})\right], \tag{11}$$

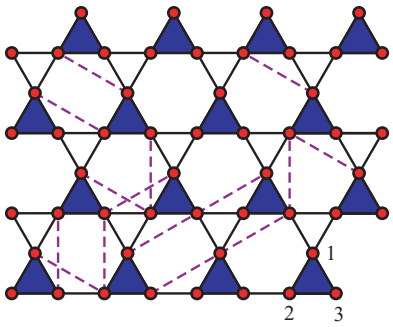


FIG. 1. (Color online) The kagome lattice with random additional NNN bonds denoted by purple dashed lines. The unit cell triangle is marked with filled triangles. Particles 1, 2, and 3 in each unit cell are marked in the bottom right unit cell.

where the summation $\sum_{\mathbf{b}}$ is over bonds connecting to one particle, and we are using a simple lattice with one particle per unit cell in this illustration. The volume of a unit cell is denoted by $v_0$.

### B. Elastic energy of the kagome lattice

The kagome lattice is a lattice with three particles per unit cell, and we shall use the following six-dimensional displacement vector to describe the deformation of the lattice:

$$\mathbf{u}_\ell = (u_{\ell,1,x}, u_{\ell,1,y}, u_{\ell,2,x}, u_{\ell,2,y}, u_{\ell,3,x}, u_{\ell,3,y}), \tag{12}$$

where $\ell$ labels the unit cell and (1,2,3) label the particles in the unit cell as in Fig. 1. To leading order in $\mathbf{u}$, the lattice energy can be expressed as the quadratic form

$$\Delta U = \frac{1}{2}\sum_{\ell,\ell'}\mathbf{u}_\ell\cdot\mathbf{D}_{\ell,\ell'}\cdot\mathbf{u}_{\ell'}, \tag{13}$$

where $\mathbf{D}$ is the $6\times 6$ dynamical matrix. This elastic energy in Fourier space is

$$\Delta U = \frac{1}{2N^2}\sum_{\mathbf{q},\mathbf{q}'}\mathbf{u}_{\mathbf{q}}\cdot\mathbf{D}_{-\mathbf{q},\mathbf{q}'}\cdot\mathbf{u}_{\mathbf{q}'}, \tag{14}$$

where the Fourier transforms are defined as

$$\mathbf{u}_{\mathbf{q}} = \sum_\ell \mathbf{u}_\ell e^{-i\mathbf{q}\cdot\mathbf{R}_{\ell 0}}, \qquad \mathbf{u}_\ell = \frac{1}{N}\sum_{\mathbf{q}}\mathbf{u}_{\mathbf{q}}e^{i\mathbf{q}\cdot\mathbf{R}_{\ell 0}}, \tag{15}$$

where $N$ is the number of unit cells. The dynamical matrix for the homogeneous kagome lattice with all nearest-neighbor (NN) bonds occupied with springs of spring constant $k$ and all NNN bonds with springs of spring constant $\kappa$ is a $6\times 6$ matrix given by

$$\mathbf{D}_{\mathbf{q},\mathbf{q}'} = N\delta_{\mathbf{q},\mathbf{q}'}\mathbf{D}_{\mathbf{q}}(k,\kappa), \qquad \mathbf{D}_{\mathbf{q}}(k,\kappa) = k\sum_{m\in\mathrm{NN}}\mathbf{B}_{m,\mathbf{q}}^{\mathrm{NN}}\mathbf{B}_{m,-\mathbf{q}}^{\mathrm{NN}} + \kappa\sum_{m\in\mathrm{NNN}}\mathbf{B}_{m,\mathbf{q}}^{\mathrm{NNN}}\mathbf{B}_{m,-\mathbf{q}}^{\mathrm{NNN}}, \tag{16}$$

where the $\mathbf{B}$ vectors and their derivation are given in Appendix A.

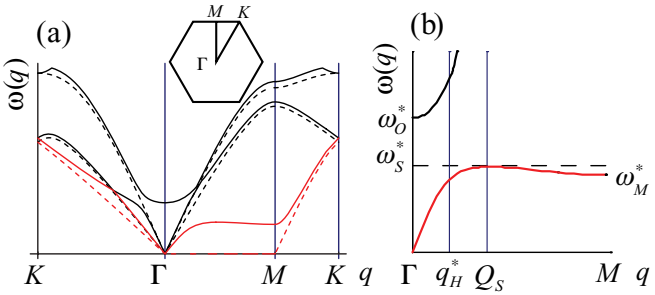


FIG. 2. (Color online) (a) Phonon dispersion along symmetry directions. The dotted lines are for $\kappa = 0$ and the solid lines are for $\kappa = 0.02$. The floppy and anomalous branches are in red. (b) Anomalous and shear modes along $\Gamma M$. Characteristic frequencies and wave numbers are also shown. Frequencies $\omega_O^*$, $\omega_S^*$, and $\omega_M^*$ are defined in the text. (From Ref. [15].)

### C. The homogeneous kagome lattice and its low-energy theory

There are six translational degrees of freedom per unit cell in the kagome lattice, giving rise to six phonon branches. Of these, three are optical branches with frequencies of order $\sqrt{k}$, two are acoustic branches with sound velocities of order $\sqrt{k}$, and one is the anomalous branch, whose frequencies along $\Gamma - M$ (see Fig. 2) in the Brillouin Zone reduce to the zero-frequency floppy modes when $\kappa \to 0$. The latter three branches, which determine the low-energy elastic theory of the kagome lattice, have modes in the space spanned by the three vectors

$$\begin{aligned} \nu_1 &= (1/\sqrt{3})(1,0,1,0,1,0), \\ \nu_2 &= (1/\sqrt{3})(0,1,0,1,0,1), \\ \nu_3 &= \left(-\frac{1}{\sqrt{3}},0,\frac{1}{2\sqrt{3}},-\frac{1}{2},\frac{1}{2\sqrt{3}},\frac{1}{2}\right), \end{aligned} \tag{17}$$

which correspond, respectively, to two translations of the whole unit cell in $x$ and $y$ directions and the rotation of the unit-cell triangle around its center. The low-energy theory is governed by the $3 \times 3$ reduced dynamical matrix obtained by integrating out the three high-energy optical branches, as shown in Appendix B.

For small momentum, $|\mathbf{q}| < q_H^* = 4\sqrt{3\kappa/k}$, the reduced dynamical matrix is simply diagonalized by longitudinal and transverse acoustic phonons (which are linear combinations of $\nu_1$ and $\nu_2$) with speeds of sound $c_L = \sqrt{3k}/4$ and $c_T = \sqrt{k}/4$ and the rotational mode with a characteristic frequency $\omega_O^* = \sqrt{6\kappa}$ at $\mathbf{q} = 0$. The bulk modulus $B$ and the shear modulus $G$ are related, respectively, to the longitudinal and transverse sound velocities through

$$c_L^2 = (B + G)/\varrho, \qquad c_T^2 = G/\varrho, \tag{18}$$

where $\varrho$ is the mass density, which, because there are three atoms per unit cell, is equal to 3 in our units. Thus, $B = 3k/8$ and $G = 3k/16$. There is only weak mixing between the rotational modes and the acoustic phonons, and the system is isotropic.

For large momentum $|\mathbf{q}| > q_H^* = 4\sqrt{3\kappa/k}$, strong mixing between the transverse acoustic modes and the rotational modes occurs, and the strong anisotropy of the isostatic

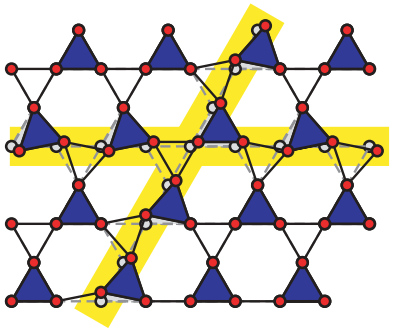

FIG. 3. (Color online) The kagome lattice and its floppy modes, with the reference state in gray and deformed state in red. Two of its floppy modes are shown in this figure marked by the yellow ribbons.

state is retrieved. The mixing is maximal along $q_x = 0$ and symmetry equivalent directions, which we refer to as the isostatic directions, and the resulting two modes are shown in Fig. 2(a). The anomalous branch, with frequency of order $\kappa$, is the lower branch of the two. In the limit of $\kappa = 0$, the lattice becomes isostatic, the isotropic region is squeezed to the origin, and the anomalous modes reduce to the isostatic floppy modes with zero frequency along $q_x = 0$ ($\Gamma M$ line in Fig. 2) and symmetry equivalent directions as depicted in Fig. 3. The name "anomalous modes" follows the nomenclature of Ref. [46], referring to the modes developed from the floppy modes as the system is moved away from the isostatic point. For a more detailed discussion of the low-energy theory of the elasticity of the kagome lattice, see Appendix B.

Of particular interest is the frequency of the anomalous modes in the vicinity of $q_x = 0$. The squared frequency of these modes can be written as

$$\omega^2(\mathbf{q}) = \omega_A^2(q_y) + c_x^2 q_x^2, \tag{19}$$

where $c_x = c_L = \sqrt{3k}/4$. The function $\omega_A^2(q_y)$ is plotted in Fig. 4. It reaches a maximum value of $(\omega_S^*)^2$ at a $2d$ saddle point at $q_y = Q_S$ and a local minimum value of $(\omega_M^*)^2$ at the zone edge $q_y = Q_M = 2\pi/\sqrt{3}$ . For small $\kappa$,

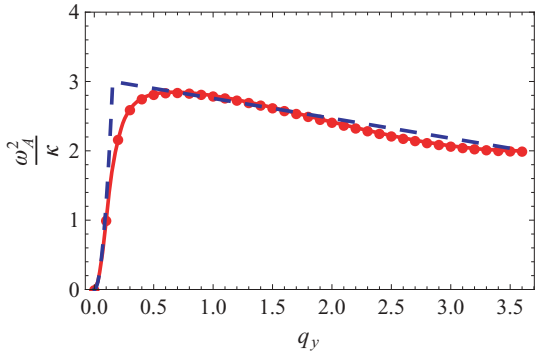


FIG. 4. (Color online) Eigenvalue of the isostatic mode along isostatic directions, for example, $q_x = 0$, for $\kappa = 5 \times 10^{-4}$. The eigenvalue of the full $6 \times 6$ dynamical matrix, $\omega^2$, normalized by $\kappa$, is denoted by the red dots, and the eigenvalue of the $3 \times 3$ reduced dynamical matrix (B2) is denoted by the red line. The blue dashed line represents the approximation (20) we used in the asymptotic calculation in the $f$ in CPA.

$Q_s \simeq 4(3\kappa/2k)^{1/4}$, $(\omega_S^*)^2 \simeq 3\kappa$, and $(\omega_M^*)^2 \simeq 2\kappa$. All of the characteristic frequencies $\omega_O^* > \omega_S > \omega_M$ are proportional to $\sqrt{\kappa}$ for small $\kappa$. $\omega_A^2(q_y)$is well approximated between $q_y = Q_S$ and $q_y = Q_M$ by

$$\omega_A^2 \approx \frac{1}{Q_M - Q_S}\left[Q_M\omega_S^2 - Q_S\omega_M^2 - q_y\left(\omega_S^2 - \omega_M^2\right)\right], \quad (20)$$

as is evident from Fig. 4. This relation will prove useful in our evaluation of integrals in our CPA analysis in Sec. III.

Lengths scaling as $\kappa^{-1/2}$ can be extracted from the phonon dispersion relations in various ways. One length is the hybridization length $l_H^*$ obtained from the hybridization wave number $q_H^* = 4\sqrt{3\kappa/k} = l_H^{*-1}$, separating the domain of predominantly transverse phonon behavior at low $q_y$ from the domain of predominantly rotation behavior at high $q_y$. Other lengths can be obtained by comparing the $c_x q_x^2$ term in $\omega^2(\mathbf{q})$ to $\omega_M^2$ and $\omega_S^2$: $q_M^* = \omega_M/c_x = l_m^{*-1} = (8/\sqrt{6})\sqrt{\kappa/k}$ and $q_S^* = \omega_S/c_x = l_S^{*-1} = 4\sqrt{\kappa/k}$. An interesting property of $\omega_A^2(q_y)$ is that the hybridization frequency $\omega_H^*$ obtained by setting $q_y = q_H^*$ in the transverse phonon frequency is identical to $\omega_S^*$: $c_T q_H^* \equiv \omega_H^* = \omega_S^*$.

One experimentally relevant quantity is the Fourier transform of the finite temperature static phonon correlation function $\mathcal{G}_{\mu,\nu}(\mathbf{l},\mathbf{l}')$,

$$\mathcal{G}_{\mu,\nu}(\mathbf{q}) = k_B T \sum_\alpha \frac{e_\mu^\alpha(-\mathbf{q})e_\nu^\alpha(\mathbf{q})}{\omega_\alpha^2(\mathbf{q})}, \quad (21)$$

where $\mu$ and $\nu$ label the basis defined in Eq. (12) of the six-dimensional space of $\mathbf{u}$, $\alpha$ labels the phonon band, and $e_\mu^\alpha(\mathbf{q})$ is the six-dimensional eigenvector associated with mode $(\alpha,\mathbf{q})$. This correlation function is a static equilibrium quantity and thus independent of phonon damping. The quantities $\omega_\alpha^2(\mathbf{q})$are merely the eigenvalues of the dynamical matrix with the zero-frequency value of the spring constant (the effective medium spring constant can depend on frequency as we discuss below in the CPA). Thus, from experimentally measured finite temperature static phonon correlation function $\mathcal{G}_{\mu,\nu}(\mathbf{l},\mathbf{l}')$, one can obtain $\omega_\alpha^2(\mathbf{q})$ from the eigenvalues of $\mathcal{G}_{\mu,\nu}(\mathbf{l},\mathbf{l}')$, and by fitting $\omega_\alpha^2(\mathbf{q})$ to Eq. (20), one will arrive at the diverging length scale $l^* \sim \kappa^{-1/2}$.[1]

## III. THE COHERENT POTENTIAL APPROXIMATION ON THE RANDOM NEARLY ISOSTATIC KAGOME LATTICE

The CPA is a widely used method in the study of disordered systems [19,33,34]. In it, a random system is mapped into an effective medium with no disorder that is described by a Green's function with a suitable self-energy that can capture the effect of the disorder average of the randomness. To achieve this, one imposes a self-consistency constraint that the effective medium Green's function perturbed by the presence of single impurity in the effective medium reduces to the effective medium Green's function when averaged over the probability distribution of the impurity. More specifically, the $T$ matrix of this perturbation vanishes upon averaging over configurations that contain and do not contain the impurity.

For the case of the nearly isostatic kagome lattice, the effective medium has all NNN bonds occupied with an effective medium spring of spring constant $\kappa_m(\mathcal{P},\omega)$, and the effective medium Green's function is identical to that of a homogeneous system with $\kappa = \kappa_m(\mathcal{P},\omega)$. The CPA procedure consists of replacing one arbitrary NNN bond with a new bond of spring constant $\kappa_s$, which takes on the value $\kappa$ with probability $\mathcal{P}$ (bond occupied) and the value 0 with probability $1 - \mathcal{P}$ (bond unoccupied). This procedure leads to a modified dynamical matrix,

$$\mathbf{D}^V = \mathbf{D} + \mathbf{V}, \quad (22)$$

where

$$\mathbf{V}_{\mathbf{q},\mathbf{q}'}(k,\kappa) = (\kappa_s - \kappa_m)\mathbf{B}_{1,\mathbf{q}}^{\mathrm{NNN}}\mathbf{B}_{1,-\mathbf{q}'}^{\mathrm{NNN}}, \quad (23)$$

where 1 represents the arbitrary NNN bond we have chosen to replace into $\kappa_s$. This form of $\mathbf{V}$ follows directly from the calculations leading to Eq. (16). It depends on the wave numbers $\mathbf{q}$ and $\mathbf{q}'$ because the perturbed system is not translationally invariant.

The phonon Green's function for the effective medium is

$$\mathbf{G}_\mathbf{q}(\omega) = [\omega^2\mathbf{I} - \mathbf{D}_\mathbf{q}]^{-1}. \quad (24)$$

In the perturbed system with one bond replaced, the Green's function becomes

$$\mathbf{G}_{\mathbf{q},\mathbf{q}'}^V(\omega) = [\omega^2\mathbf{I} - \mathbf{D}^V]_{\mathbf{q},\mathbf{q}'}^{-1} \quad (25)$$

and is no longer translationally invariant. This Green's function can be expanded for small $\mathbf{V}$,

$$\begin{aligned}\mathbf{G}_{\mathbf{q},\mathbf{q}'}^V &= (\mathbf{I} - \mathbf{G}\cdot\mathbf{V})_{\mathbf{q},\mathbf{q}'}^{-1}\cdot\mathbf{G}_{\mathbf{q}'} \\ &\simeq N\delta_{\mathbf{q},\mathbf{q}'}\mathbf{G}_\mathbf{q} + \mathbf{G}_\mathbf{q}\cdot\mathbf{V}_{\mathbf{q},\mathbf{q}'}\cdot\mathbf{G}_{\mathbf{q}'} \\ &\quad + \frac{1}{N}\sum_{\mathbf{q}_1}\mathbf{G}_\mathbf{q}\cdot\mathbf{V}_{\mathbf{q},\mathbf{q}_1}\cdot\mathbf{G}_{\mathbf{q}_1}\cdot\mathbf{V}_{\mathbf{q}_1,\mathbf{q}'}\cdot\mathbf{G}_{\mathbf{q}'} + \cdots, \end{aligned} \quad (26)$$

where we have dropped the frequency $\omega$ dependence, which is the same for every $\mathbf{G}$ and $\mathbf{V}$. This series can be written as

$$\mathbf{G}_{\mathbf{q},\mathbf{q}'}^V = N\delta_{\mathbf{q},\mathbf{q}'}\mathbf{G}_\mathbf{q} + \mathbf{G}_\mathbf{q}\cdot\mathbf{T}_{\mathbf{q},\mathbf{q}'}\cdot\mathbf{G}_{\mathbf{q}'}, \quad (27)$$

where

$$\begin{aligned}\mathbf{T}_{\mathbf{q},\mathbf{q}'} \equiv \mathbf{V}_{\mathbf{q},\mathbf{q}'} &+ \frac{1}{N}\sum_{\mathbf{q}_1}\mathbf{V}_{\mathbf{q},\mathbf{q}_1}\cdot\mathbf{G}_{\mathbf{q}_1}\cdot\mathbf{V}_{\mathbf{q}_1,\mathbf{q}'} \\ &+ \frac{1}{N^2}\sum_{\mathbf{q}_1,\mathbf{q}_2}\mathbf{V}_{\mathbf{q},\mathbf{q}_1}\cdot\mathbf{G}_{\mathbf{q}_1}\cdot\mathbf{V}_{\mathbf{q}_1,\mathbf{q}_2}\cdot\mathbf{G}_{\mathbf{q}_2}\cdot\mathbf{V}_{\mathbf{q}_2,\mathbf{q}'} \\ &+ \cdots \end{aligned} \quad (28)$$

is the $T$ matrix expressed in the wave number basis.

In the CPA, the effective medium spring constant $\kappa_m$ is determined by requiring that the average value of $\mathbf{G}_{\mathbf{q},\mathbf{q}'}^V$ be equal to $N\delta_{\mathbf{q},\mathbf{q}'}\mathbf{G}_\mathbf{q}$ or equivalently that the disorder average of the $T$ matrix vanish:

$$\mathcal{P}\mathbf{T}|_{\kappa_s=\kappa} + (1-\mathcal{P})\mathbf{T}|_{\kappa_s=0} = 0. \quad (29)$$

[1]Our prescription, which unambiguously produces a length scale for uniform or randomly diluted periodic lattices, has not to our knowledge yielded a length scale for the jamming problem, whose lattice is not periodic.

The evaluation of the $T$ matrix is simplified by the following identity:

$$\frac{1}{N}\sum_{\mathbf{q}_1}\mathbf{V}_{\mathbf{q},\mathbf{q}_1}\cdot\mathbf{G}_{\mathbf{q}_1}\cdot\mathbf{V}_{\mathbf{q}_1,\mathbf{q}'}$$

$$=(\kappa_s-\kappa_m)^2\mathbf{B}^{\mathrm{NNN}}_{1,\mathbf{q}} \tag{30}$$

$$\times\frac{1}{N}\left(\sum_{\mathbf{q}_1}\mathbf{B}^{\mathrm{NNN}}_{1,-\mathbf{q}_1}\cdot\mathbf{G}_{\mathbf{q}_1}\cdot\mathbf{B}^{\mathrm{NNN}}_{1,\mathbf{q}_1}\right)\mathbf{B}^{\mathrm{NNN}}_{1,-\mathbf{q}'} \tag{31}$$

$$=-(\kappa_s-\kappa_m)\mathbf{V}_{\mathbf{q},\mathbf{q}'}f(\kappa_m,\omega), \tag{32}$$

where

$$f(\kappa_m,\omega)=-v_0\int_{1\mathrm{BZ}}\frac{d^2\mathbf{q}}{4\pi^2}\,\mathbf{B}^{\mathrm{NNN}}_{1,-\mathbf{q}}\cdot\mathbf{G}_{\mathbf{q}}(\omega)\cdot\mathbf{B}^{\mathrm{NNN}}_{1,\mathbf{q}}, \tag{33}$$

with $v_0=\sqrt{3}/2$ the area of the unit cell in real space and $4\pi^2/v_0=8\pi^2/\sqrt{3}$ is the area of the first Brillouin zone in reciprocal space. The integral is over the first Brillouin zone. The Green's function $\mathbf{G}_{\mathbf{q}}(\omega)$ is the phonon Green's function in the effective medium so it depends on $\kappa_m$. Using these relations in Eq. (28) gives

$$\mathbf{T}_{\mathbf{q},\mathbf{q}'}=\frac{\mathbf{V}_{\mathbf{q},\mathbf{q}'}}{1+(\kappa_s-\kappa_m)f(\kappa_m,\omega)}. \tag{34}$$

Thus, the self-consistency equation (29) requires that

$$f(\kappa_m,\omega)\kappa_m^2-[1+\kappa f(\kappa_m,\omega)]\kappa_m+\mathcal{P}\kappa=0, \tag{35}$$

from which one can solve for the effective medium NNN spring constant $\kappa_m$ for any given $\mathcal{P}$ and $\omega$. The form of this solution at small $\kappa_m$ depends on the behavior of the function $f(\kappa_m,\omega)$ at small $\kappa_m$, which is in turn determined by the form of the anomalous mode along the $q_x=0$ and other isostatic directions. Details of the calculation of $f(\kappa_m,\omega)$ are presented in Appendix B.

In the following discussion, unless otherwise stated, we use reduced units with $k=1$ and lattice constant $a=1$, and thus unitless spring constants, elastic moduli, and frequencies: $\kappa/k\to\kappa$, $Ga^2/k\to G$, and $\omega/\sqrt{k}\to\omega$, respectively.

## IV. RESULTS AND DISCUSSION

### A. CPA solution at zero frequency: Static response

We first consider the case of $\omega=0$, which characterizes the static response of the system. For small $\mathcal{P}$, we expect that the effective medium spring constant $\kappa_m$ also to be small and that we can, therefore, ignore the $f(\kappa_m,\omega)\kappa_m^2$ term in the CPA self-consistency equation (35). Using the asymptotic small $\kappa_m$ limit $f(\kappa_m,0)=ß/\sqrt{\kappa_m}$, where $ß=5(1-\sqrt{2/3})$, derived in Appendix B [Eq. (B13)], we obtain the equation

$$\kappa_m+ß\kappa\sqrt{\kappa_m}-\mathcal{P}\kappa=0, \tag{36}$$

determining $\kappa_m$ at small $\mathcal{P}$. The solution to this equation,

$$\kappa_m(\mathcal{P},0)=\left[\frac{-ß\kappa+\sqrt{ß^2\kappa^2+4\mathcal{P}\kappa}}{2}\right]^2, \tag{37}$$

has two limits,

$$\kappa_m(\mathcal{P},0)\simeq\begin{cases}\mathcal{A}\mathcal{P}^2 & \text{if } \mathcal{P}\ll(ß^2/4)\kappa,\\ \mathcal{P}\kappa & \text{if } \mathcal{P}\gg(ß^2/4)\kappa,\end{cases} \tag{38}$$

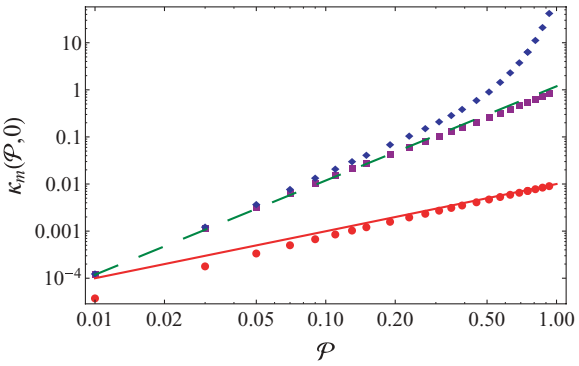


FIG. 5. (Color online) CPA solution at zero frequency. Data points show the numerical solution $\kappa_m$ as a function of $\mathcal{P}$ at $\omega=0$ of the CPA self-consistency equation (35) with the full $6\times6$ dynamical matrix. NNN bond spring constant $\kappa=10^{-2},10^{0},10^{2}$ are shown as red dots, purple squares, and blue diamonds, respectively. Also shown are the nonaffine ($\kappa_m=A\mathcal{P}^2$) and affine ($\kappa_m=\mathcal{P}\kappa$ at $\kappa=10^{-2}$) limits as a green dashed line and a red dotted line, respectively. At large $\mathcal{P}$ the numerical solution, especially the one for $\kappa=10^2$ deviate significantly from the nonaffine limit form because Eq. (36) is an approximation at small $\mathcal{P}$ by ignoring the highest-order term in Eq. (35).

where $\mathcal{A}=1/ß^2=3(5+2\sqrt{6})/25$. In the first case, $\kappa\sqrt{\kappa_m}\gg\kappa_m$, and the solution for $\kappa_m$ is obtained by ignoring the first term in Eq. (36); in the second case, the opposite is true, and $\kappa_m$ is obtained by ignoring the second term in this equation. In the second case, every NNN bond distorts in the same way under stress, and response is affine. In the first case, $\kappa_m=\mathcal{A}\mathcal{P}^2\ll\mathcal{P}\kappa$, indicating that the response is nonaffine with local rearrangements in response to stress. Within the CPA, this result emerges because of the divergent elastic response encoded in $\mathbf{G}$ [and $f(\kappa_m,0)$] as $\kappa_m\to0$ (see Appendix B). The nonaffine regime arises when NNN springs are strong enough for the second term in Eq. (36) to dominate the first. As $\kappa$ approaches zero at fixed $\mathcal{P}$, distortions produced by the extra bond decrease and the nonaffine regime becomes vanishingly small. Numerical solutions of the CPA self-consistency equation (35) with the full $6\times6$ dynamical matrix are plotted in Fig. 5, along with a comparison to the analytical solution (37) and the two asymptotic forms in Eq. (38).

The effective NNN spring constant $\kappa_m$ in both the square [16] and kagome lattices exhibit an affine $G\sim\mathcal{P}$ to nonaffine $G\sim\mathcal{P}^2$ crossover with decreasing $\mathcal{P}$. The effects of this crossover are, however, different in the two cases. In the square lattice, the shear modulus $G\equiv C_{44}$ is equal to $\kappa_m$, and as a result, the macroscopic shear response exhibits this crosser. In the kagome lattice, the shear modulus is proportional to the NN spring constant $k$ rather than $\kappa$, and the macroscopic elastic response does not exhibit the affine to nonaffine crossover. The crossover appears instead in the anomalous mode that reduces to the floppy modes shown in Fig. 3 when $\kappa_m\to0$.

Length and frequency scales can be extracted in the static limit much as they were extracted in the homogeneous case discussed in Sec. II. The finite temperature static phonon correlation function $\mathcal{G}$ is the inverse of the dynamical matrix evaluated at $\omega=0$, whose eigenvalues and eigenvectors are identical to those of the homogeneous case with $\kappa$ replaced

by $\kappa_m \equiv \kappa_m(\mathcal{P},0)$. The eigenvalues allow us to identify frequencies by taking the square roots of the appropriate eigenvalues of $\mathbf{D}$:

$$\omega_O^* = \sqrt{6\kappa_m} > \omega_S^* = \sqrt{3\kappa_m} > \omega_M^* = \sqrt{2\kappa_m}. \quad (39)$$

Unlike the situation in homogeneous lattices, these frequencies are not equal to any physical dynamical-mode frequency of the system. They do, however, provide information about the static properties of the phonon correlation function $\mathcal{G}$ that could, in principle, be measured at finite temperature via scattering or particle tracking experiment. They also lead to diverging lengths just as they do in the homogeneous case:

$$l^* \equiv l_H^* = \frac{1}{\sqrt{3}} l_S^* = \sqrt{2}\, l_M^* = \frac{1}{4\sqrt{3\kappa_m}} = \frac{1}{\sqrt{3\mathcal{A}}} \frac{1}{\Delta z}. \quad (40)$$

### B. CPA solution at finite frequency: Dynamic response and damping

For finite frequency $\omega$, the effective medium spring constant is complex, $\kappa_m(\mathcal{P},\omega) = \kappa_m'(\mathcal{P},\omega) - i\kappa_m''(\mathcal{P},\omega)$, where the imaginary part $\kappa_m''(\mathcal{P},\omega)$, which describes damping of phonons in this random network, is odd in $\omega$ and positive for $\omega > 0$. From the analysis for the static limit $\omega = 0$, we see that the interesting case is the nonaffine regime with $\mathcal{P} \ll (ß^2/4)\kappa$, in which the self-consistency equation (36) simplifies to

$$f(\kappa_m,\omega)\kappa_m = \mathcal{P}. \quad (41)$$

In the static limit, $f(\kappa_m,0) \sim \kappa_m^{-1/2}$ is singular in the $\kappa_m \to 0$ limit. As we show in Appendix B, at finite frequency, $f(\kappa_m,\omega) \sim [\sqrt{(3\kappa_m - \omega^2)/\kappa_m} - \sqrt{(2\kappa_m - \omega^2)/\kappa_m}]/\kappa_m$, which leads to

$$\kappa_m(\mathcal{P},\omega) = \frac{3\mathcal{P}^2}{25}\left(5 + 2\sqrt{6}\sqrt{1 - \frac{25\omega^2}{18\mathcal{P}^2}}\right), \quad (42)$$

as depicted in Fig. 6. Taking $\omega = 0$, this solution reduces to the zero-frequency solution [Eq. (38)] in the nonaffine limit. Equation (42) develops an imaginary part when $|\omega| > 2\sqrt{3}\mathcal{P}/5$, which, as we discussed earlier, must be negative for $\omega > 0$. It is straightforward to see that this solution satisfies the scaling form $\kappa_m(\mathcal{P},\omega) = \kappa_m(\mathcal{P},0)h(\omega/\omega^*)$, as does the CPA effective NNN spring constant in the square lattice [16]. This solution shows a rapid increase of damping beyond a characteristic frequency,

$$\omega_D^* = \frac{2\sqrt{3}\mathcal{P}}{5}, \quad (43)$$

marking another characteristic frequency that scales also as $\mathcal{P}$.

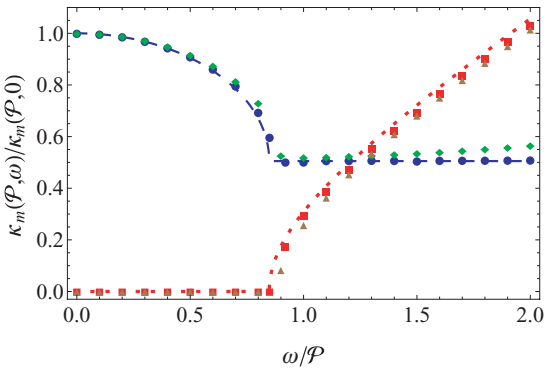


FIG. 6. (Color online) CPA solution at finite frequency for $\mathcal{P} = 0.01$ and $\mathcal{P} = 0.05$. The numerical solution to Eq. (35) with the full $6 \times 6$ dynamical matrix is shown as the data points. Blue circles and red squares represent real and (negative of) imaginary parts of $\kappa_m$ at $\mathcal{P} = 0.01$, respectively, and green diamonds and brown triangles represent the real and (negative of) imaginary parts of $\kappa_m$ at $\mathcal{P} = 0.05$, respectively. The asymptotic form (42) is shown as the blue (real) and red (negative of imaginary) lines. In this plot frequency is rescaled by $\mathcal{P}$, and the effective medium spring constant $\kappa_m$ is rescaled by its value at zero frequency, which is real.

Numerical solutions of the CPA self-consistency equation (35) using the full $6 \times 6$ dynamical matrix is also shown in Fig. 6. We see that the asymptotic form (42) captures the solution fairly well.

This special behavior of the imaginary part of the effective medium spring constant $\kappa_m$ is related to the phonon spectrum of the kagome lattice. As we discussed in Sec. II, at low frequencies, there is only very weak mixing between the rotational branch, which is strongly affected by the NNN bonds, and the acoustic phonon branches, which are only very weakly affected by the NNN bonds. As a result, the damping to the acoustic phonons is very weak. On the other hand, at frequencies greater that $\omega_D^*$, the transverse phonons scatter strongly from the anomalous modes, and there is a rapid increase in their damping. The weak scattering below $\omega_D^*$ is not captured by the asymptotic form (42) for small $\kappa_m$ because the function $\kappa_m(\mathcal{P},\omega)$ in Eq. (42) was obtained using the dominant small $\kappa_m$ limit of the integral $f(\kappa_m,\omega)$. There are, however, contributions to this integral that do not diverge and that contribute a subdominant imaginary part to $\kappa_m$, even when $\omega < \omega_D^*$, that is, of order $\mathcal{P}^3\omega^2$ at small $\omega$ corresponding to Rayleigh scattering. More discussion is included in Appendix B.

In the homogeneous case, the eigenvalues of the dynamical matrix lead naturally to the identification of characteristic frequencies $\omega_S^*$ and $\omega_M^*$ that vanish as $\sqrt{\kappa}$ in the limit of $\kappa \to 0$. In the random case, we have to deal with both the frequency dependence of $\kappa_m(\mathcal{P},\omega)$ and the fact that it is a complex number, and we must ask whether these frequencies have any real meaning. As discussed in Sec. II C, we can extract frequencies from the static dynamical matrix in exactly the same way that we did for the homogeneous case, and they satisfy

$$\omega_O^* = 3.85\omega_D^* > \omega_S^* = 2.72\omega_D^* > \omega_M^* = 2.22\omega_D^* > \omega_D^*. \quad (44)$$

Thus, all of these frequencies are greater than the frequency $\omega_D$. As a result, the signatures in the phonon dispersion relation including hybridization and the saddle point giving rise to the logarithmic van Hove singularity in the density of states of the uniform NNN kagome lattice are washed out by the strong scattering, as is shown in Fig. 7.

### C. Phonon density of states

The phonon density of states (DOS) can be calculated from the retarded Green's function through

$$\rho(\omega) = -\frac{1}{\pi}\mathrm{Tr}\,\mathrm{Im}\mathbf{G}\,(\mathbf{q},\omega), \quad (45)$$

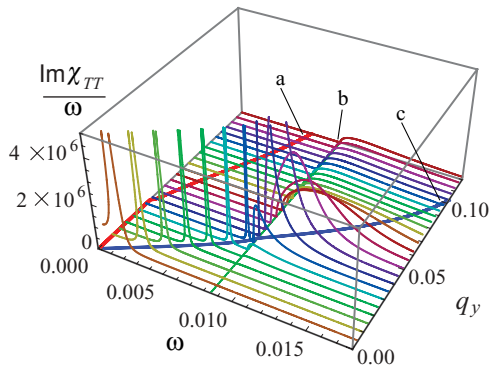


FIG. 7. (Color online) Scattering of phonons characterized using the imaginary part of the transverse component of the phonon response function divided by frequency $\mathrm{Im}\chi_{TT}(\mathbf{q},\omega)/\omega$ as a function of $\omega$ for various values of $q_y$ (we took $q_x = 0$ to follow the isostatic $\Gamma M$ direction). The green line (b) in the bottom plane marks $\omega_D^*$, the blue (c) and red (a) lines marks the solution $\omega'$ and $\omega''$ of the equation $\omega^2 - \omega_A[\mathbf{q},\kappa_m(\mathcal{P},\omega)]^2 = 0$, which solves for the pole of the Green's function for the anomalous branch. The derivation of $\omega_A$ is shown in Appendix B.

where the trace is over both momentum $\mathbf{q}$ and the phonon branches. Using this we obtain the phonon DOS of the effective medium plotted in Fig. 8. For comparison, we also show the phonon DOS of a periodic kagome lattice with the NNN spring constant equal to $\kappa_m(\mathcal{P},0)$, which is real valued.

For small frequencies, at which the imaginary part of the CPA solution $\kappa_m(\mathcal{P},\omega)$ is very small, the two DOS are very close and can be fitted nicely by the Debye-like total DOS of the transverse and the longitudinal phonons,

$$\rho_s(\omega) = \frac{\omega}{(4\pi/\sqrt{3})c_L^2} + \frac{\omega}{(4\pi/\sqrt{3})c_T^2}, \tag{46}$$

where $c_L^2 = 3k/16$ and $c_T^2 = k/16$ are, respectively, the longitudinal and transverse speed of sound (we have taken $k = 1$ as stated earlier).

At the critical frequency $\omega_D^*$, the imaginary part of $\kappa_m(\mathcal{P},\omega)$ increases rapidly, inducing a rapid increase of the phonon DOS. On the other hand, the periodic lattice exhibit a jump in DOS at $\omega_M^* = \sqrt{2\kappa_m(\mathcal{P},0)}$ corresponding to the minimum of the phonon dispersion relations at the edge of the first Brillouin zone. At $\omega_S^* = \sqrt{3\kappa_m(\mathcal{P},0)}$ the DOS of the periodic lattice has a logarithmic singularity, corresponding to the saddle point of the phonon dispersion at $Q_S \simeq 4(3\kappa_m/2k)^{1/4}$ on the isostatic directions [15]. For the CPA effective medium, this singularity is totally washed out due to the strong damping beyond $\omega_D^*$, which is similar to the case of the square lattice [16].

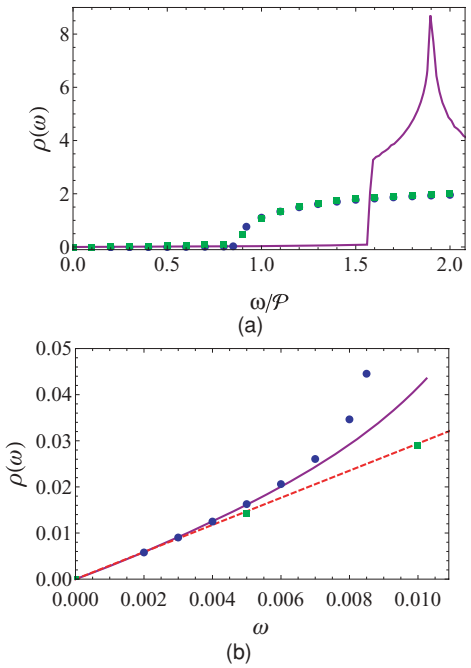


FIG. 8. (Color online) (a) The phonon DOS at $\mathcal{P} = 0.01$ (blue circles) and $\mathcal{P} = 0.05$ (green squares) of the CPA effective medium and the pure kagome lattice with the NNN spring constant equal to the zero-frequency effective medium value $\kappa_m(\mathcal{P},\omega)$ for $\mathcal{P} = 0.01$ (purple line). The frequency is rescaled by $\mathcal{P}$. (b) The phonon DOS at small frequency for CPA effective medium [color scheme the same as in (a)]. The Debye DOS defined in Eq. (46) is also shown as the red dashed line.

### D. Phonon scattering and the Ioffe-Regel limit

From the CPA solution at finite frequency, we identified a frequency scale $\omega_D^*$ beyond which phonon scattering rapidly increased. In this section we examine the scattering of phonons in more detail.

The scattering of the transverse phonons is characterized by the imaginary part of the phonon response function projected to the transverse direction $\mathrm{Im}\chi_{TT}(\mathbf{q},\omega)$. The phonon response function is defined as

$$\chi_{\mu,\nu}(\ell,t;\ell',t') \equiv \frac{\delta u_\mu(\ell,t)}{\delta F_\nu(\ell',t')}, \tag{47}$$

where $t$ and $t'$ label time and $\mu$ and $\nu$ label the basis defined in Eq. (12) of the six-dimensional space of $\mathbf{u}$. This response function is related to the phonon Green's function through $\chi = -\mathbf{G}$. The imaginary part of the transverse component of this response function $\mathrm{Im}\chi_{TT}(\mathbf{q},\omega)$ characterizes the scattering of the transverse phonon by disorder. $\mathrm{Im}\chi_{TT}(\mathbf{q},\omega)$ is calculated for small momentum and frequency using the asymptotic CPA solution (42) and shown in Fig. 7. Also shown in the figure is the frequency at which the phonon Green's function of the anomalous branch has a complex pole, which is solved from the equation $\omega^2 - \omega_A[\mathbf{q},\kappa_m(\mathcal{P},\omega)]^2 = 0$, which characterizes the dynamic dispersion relation. We use the form of $\omega_A$ as defined in Appendix B for this calculation. Below $\omega_D^*$, the response function has Dirac-$\delta$ peaks at the frequencies determined by the transverse phonon dispersion relation $\omega = c_T q_y$. Above $\omega_D^*$ the imaginary part $\omega''$ increases rapidly, and the phonon peaks progressively broaden, showing that the transverse phonon is no longer a good eigenstate of the system. Furthermore, the characteristic frequencies for the hybridization of the transverse phonon and the rotational phonon into the anomalous mode and of the van Hove singularities in the DOS are greater than $\omega_D^*$, and as a result, these phenomena are washed out by the strong scattering. As a result, $\omega_O^*$, $\omega_S^*$, $\omega_M^*$ no longer play a meaningful role in the dynamic response function.

The strength of the scattering can be characterized by the Ioffe-Regel (IR) limit, which states that the plane-wave

states are no longer well defined if the mean-free path $l_{\rm mfp}$ is comparable to or less than the phonon wavelength $\lambda$. An equivalent condition is that the relaxation time becomes comparable to the period of the wave, that is, $\omega'' \sim \omega'$. The solution for the positions of the complex poles of the Green's function of the anomalous branch $\omega^2 - \omega_A[\mathbf{q},\kappa_m(\mathcal{P},\omega)]^2 = 0$ shows that the imaginary part $\omega''$ becomes comparable to the real part $\omega'$ not far beyond $\omega_D^*$ and that $\omega_{\rm IR}^* \sim \omega_D^* \sim \Delta z$. The associated IR length scale can be derived from $\omega_D^*$ and $c_T$ to be of order $l_{\rm IR} \sim \sqrt{k/\kappa_m} \sim \Delta z^{-1}$.

This IR length scale differs from that in jammed solids, $l_d \sim \Delta z^{-1/2}$ as derived in Refs. [47,48] (called $l_s$ in Ref. [31]). This discrepancy can be attributed to the different scaling of the shear modulus $G$. In the kagome lattice, the shear modulus $G$ is proportional to $k$ and thus scales as $\Delta z^0$, whereas in jammed solids $G \sim \Delta z$. Thus, the transverse speeds of sound scales as $(\Delta z)^0$ and $(\Delta z)^{1/2}$ in these two cases, respectively. In both cases, the frequency beyond which plane-wave states are strongly scattered is $\omega^* \sim \Delta z$. Therefore, the scattering length scales, $c_T/\omega^*$, are, respectively, $l^* \sim (\Delta z)^{-1}$ and $l_d \sim (\Delta z)^{-1/2}$ in the kagome lattice and jammed solids.

### E. Comparison between different random nearly isostatic systems

Up to now, three examples of random nearly isostatic systems have been studied, including the random nearly isostatic square lattice, the random nearly isostatic kagome lattice discussed in this paper, and jammed solids near point $J$. In all cases, the characteristic frequency for the onset of the anomalous mode plateau $\omega^* \sim \Delta z$ and the isostatic length scale $l^* \sim (\Delta z)^{-1}$. On the other hand, the scaling of elastic moduli in the three cases are different because of different *network architecture*: In the square lattice $G \sim \kappa_m \sim (\Delta z)^2$ and $B \sim k \sim (\Delta z)^0$, in the kagome lattice $G, B \sim k \sim (\Delta z)^0$, and in jammed solids $G \sim \Delta z$ and $B \sim k \sim (\Delta z)^0$ (a jump from zero to finite value at point $J$). As a result, the scattering length scales are also different. The square lattice is anisotropic, and we studied the scattering of the $u_x$ vibrations along $q_y$ direction and found that the scattering length corresponded to the point $M$ in the first Brillouin zone, $q_y = \pi$, or $l_{x,\rm IR} = a$. In the kagome lattice $l_{\rm IR} \sim c_T/\omega^* \sim (\Delta z)^{-1}$. In jammed solids, the IR length scale $l_d \sim c_T/\omega^* \sim (\Delta z)^{-1/2}$.

In Ref. [31], Wyart studied transport properties of amorphous solids modeled by an isotropic random network near its percolative rigidity threshold. In this system, both $B$ and $G$ vanish as $\Delta z$, and the crossover frequency between plane-wave and strongly scattered states is $\omega^* \sim \Delta z$. Both the longitudinal and the transverse sound velocities scale as $(\Delta z)^{1/2}$, and the IR length $l_{\rm IR} \sim c_{L,T}/\omega^*$ scales as $(\Delta z)^{-1/2}$ for both modes. By ignoring the $i\omega^3$ term, which is a reflection of Rayleigh scattering in three dimensions, the CPA self-consistency equation for low frequency in Ref. [31], Eq. (7), can be rewritten in the form

$$k_M^2 - (\Delta z) k_M + \omega^2 = 0. \tag{48}$$

The solution to this equation,

$$k_M = \frac{\Delta z}{2}\left(1 + \sqrt{1 - \frac{4\omega^2}{\Delta z^2}}\right), \tag{49}$$

has a form very similar to the that of the effective medium NNN spring constant $\kappa_m$ in the kagome lattice, as shown in Eq. (42). Although $k_M(\omega = 0) \sim \Delta z$ in the amorphous solid and $\kappa_m(\omega = 0) \sim (\Delta z)^2$ in the kagome lattice scale differently with $\Delta z$, the frequency dependence of $k_M(\omega)/k_M(\omega = 0)$ and $\kappa_m(\omega)/\kappa_m(\omega = 0)$ are almost identical: They are both of the form $a + b\sqrt{1 - (\omega/\omega_D^*)^2}$, where $a$ and $b$ are constants and $\omega_D \sim \Delta z$. The $\omega^3$ term ignored in the preceding analysis leads to Rayleigh scattering, $l_d \sim \omega^{-4}$ at small $\omega$. In the case of the kagome lattice, the subdominant terms in $f$ (as discussed in Sec. IV B) contribute $\omega^2$ in $\kappa_m''$, and lead to Rayleigh scattering $l_d \sim \omega^{-3}$. The difference in the exponent in these two cases is due to different spatial dimension.

To summarize, we examined the random nearly isostatic kagome lattice via the CPA and we obtained effective medium NNN spring constant $\kappa_m$ that scales with the occupancy probability $\mathcal{P} \sim \Delta z$ of the NNN bonds as $\mathcal{P}^2$ at small $\mathcal{P}$. Below the characteristic frequency $\omega_D^* \sim \mathcal{P}$, there is only weak damping of acoustic phonons arising from Rayleigh scattering, whereas above $\omega_D^*$ scattering increases rapidly and the system shows proximity to the IR limit. We compare the kagome lattice to other nearly isostatic systems including the square lattice, jammed solids near point $J$, and a model random isotropic network [31]. The characteristic frequency scale $\omega^* \sim \Delta z$, marking both the onset of the plateau of the anomalous modes and the strong scattering of plain wave states, is found to be a universal property of all of these systems. The elastic modulus $G, B$ and thus the transport length scale depends on the *network architecture* and are not universal.


## ACKNOWLEDGMENT

This work was supported in part by Grant No. NSF-DMR-0804900.


## APPENDIX A: THE DYNAMICAL MATRIX OF THE KAGOME LATTICE

To construct the dynamical matrix of the kagome lattice, we use the form of the elastic energy given in Eq. (7). Because we consider the reference state of all bonds at their rest length, we have $f_b = 0$; thus, there is only projection of $u$ onto the direction along the bond. We first consider the case of a simple lattice with one particle in each unit cell and rewrite Eq. (7) as

$$\begin{aligned}\Delta U &= \sum_b \frac{k_b}{2}\left[\left(\mathbf{u}_{\ell_1} - \mathbf{u}_{\ell_2}\right)\cdot \mathbf{e}_{\ell_1\ell_2}\right]^2 \\ &= \sum_{\ell,\ell'}\sum_b \frac{k_b}{2}\mathbf{u}_\ell \cdot \mathbf{e}_{\ell_1\ell_2}\left(\delta_{\ell,\ell_1} - \delta_{\ell,\ell_2}\right) \\ &\quad \times \left(\delta_{\ell',\ell_1} - \delta_{\ell',\ell_2}\right)\mathbf{e}_{\ell_1\ell_2}\cdot \mathbf{u}_{\ell'},\end{aligned} \tag{A1}$$

where $\ell_1, \ell_2$ labels the two particles connected by the bond $b$. Thus, the dynamical matrix $\mathbf{D}$, as defined in Eq. (13), is given by

$$\mathbf{D}_{\ell,\ell'} = \sum_b k_b \mathbf{e}_{\ell_1\ell_2}\left(\delta_{\ell,\ell_1} - \delta_{\ell,\ell_2}\right)\left(\delta_{\ell',\ell_1} - \delta_{\ell',\ell_2}\right)\mathbf{e}_{\ell_1\ell_2}. \tag{A2}$$

It is convenient to express the dynamical matrix in momentum space via the Fourier transform defined in Eq. (15)

$$\begin{aligned}\mathbf{D}_{\mathbf{q},\mathbf{q}'} &= \sum_{\ell,\ell'} e^{-i\mathbf{q}\cdot\mathbf{r}_\ell + i\mathbf{q}'\cdot\mathbf{r}_{\ell'}}\mathbf{D}_{\ell,\ell'} \\ &= \sum_{\ell,\ell'} e^{-i\mathbf{q}\cdot\mathbf{r}_\ell + i\mathbf{q}'\cdot\mathbf{r}_{\ell'}} \sum_{\ell_1}{\sum_{\ell_2}}' k_b \mathbf{e}_{\ell_1\ell_2} \\ &\quad \times \left(\delta_{\ell,\ell_1} - \delta_{\ell,\ell_2}\right)\left(\delta_{\ell',\ell_1} - \delta_{\ell',\ell_2}\right)\mathbf{e}_{\ell_1\ell_2} \\ &= N\delta_{\mathbf{q},\mathbf{q}'} \sum_{\mathbf{b}} k_{\mathbf{b}}(1 - e^{-i\mathbf{q}\cdot\mathbf{b}}) \\ &\quad \times (1 - e^{i\mathbf{q}\cdot\mathbf{b}})\mathbf{e}_{\mathbf{b}}\mathbf{e}_{\mathbf{b}}, \end{aligned} \tag{A3}$$

where the $'$ above the summation of $\ell_2$ denotes a summation over particles connected to $\ell_1$, and $\mathbf{b} = \mathbf{r}_{\ell'} - \mathbf{r}_\ell$ represents the bonds connected to an arbitrary particle (note the difference from $b$ in the previous equation, which represents all bonds in the system). One can define the dynamical matrix for translational invariant system as

$$\begin{aligned}\mathbf{D}_{\mathbf{q},\mathbf{q}'} &= N\delta_{\mathbf{q},\mathbf{q}'}\mathbf{D}_{\mathbf{q}}, \\ \mathbf{D}_{\mathbf{q}} &= \sum_{\mathbf{b}} k_{\mathbf{b}}(1 - e^{-i\mathbf{q}\cdot\mathbf{b}})(1 - e^{i\mathbf{q}\cdot\mathbf{b}})\mathbf{e}_{\mathbf{b}}\mathbf{e}_{\mathbf{b}} \\ &= \sum_m k_m \mathbf{B}_{m,\mathbf{q}}\mathbf{B}_{m,-\mathbf{q}}, \end{aligned} \tag{A4}$$

where the summation $m$ is over bonds connected to an arbitrary particle, and the vector

$$\mathbf{B}_{m,\mathbf{q}} = (1 - e^{-i\mathbf{q}\cdot\mathbf{b}_m})\mathbf{e}_{\mathbf{b}_m} \tag{A5}$$

is a convenient way to express the dynamical matrix.

For the kagome lattice, which has three particles per unit cell, one needs to modify the preceding construction of the dynamical matrix, and in the basis of

$$\mathbf{u}_\ell = (u_{\ell,1,x}, u_{\ell,1,y}, u_{\ell,2,x}, u_{\ell,2,y}, u_{\ell,3,x}, u_{\ell,3,y}), \tag{A6}$$

with particles 1,2,3 labeled as in Fig. 1, the dynamical matrix can be expressed as

$$\begin{aligned}\mathbf{D}_{\mathbf{q},\mathbf{q}'} &= N\delta_{\mathbf{q},\mathbf{q}'}\mathbf{D}_{\mathbf{q}}(k,\kappa), \\ \mathbf{D}_{\mathbf{q}}(k,\kappa) &= k\sum_{m\in\mathrm{NN}} \mathbf{B}^{\mathrm{NN}}_{m,\mathbf{q}}\mathbf{B}^{\mathrm{NN}}_{m,-\mathbf{q}} \\ &\quad + \kappa\sum_{m\in\mathrm{NNN}} \mathbf{B}^{\mathrm{NNN}}_{m,\mathbf{q}}\mathbf{B}^{\mathrm{NNN}}_{m,-\mathbf{q}}, \end{aligned} \tag{A7}$$

with the $\mathbf{B}$ vectors for NN bonds for each unit cell (each bond is counted once)

$$\mathbf{B}^{\mathrm{NN}}_{1,\mathbf{q}} = \left(-\frac{1}{2}, -\frac{\sqrt{3}}{2}, \frac{1}{2}, \frac{\sqrt{3}}{2}, 0, 0\right),$$

$$\mathbf{B}^{\mathrm{NN}}_{2,\mathbf{q}} = (0,0,1,0,-1,0),$$

$$\mathbf{B}^{\mathrm{NN}}_{3,\mathbf{q}} = \left(\frac{1}{2}, -\frac{\sqrt{3}}{2}, 0, 0, -\frac{1}{2}, \frac{\sqrt{3}}{2}\right),$$

$$\mathbf{B}^{\mathrm{NN}}_{4,\mathbf{q}} = \left(-\frac{1}{2}, -\frac{\sqrt{3}}{2}, \frac{1}{2}e^{-i(\frac{1}{2}q_x + \frac{\sqrt{3}}{2}q_y)}, \frac{\sqrt{3}}{2}e^{-i(\frac{1}{2}q_x + \frac{\sqrt{3}}{2}q_y)}, 0, 0\right), \tag{A8}$$

$$\mathbf{B}^{\mathrm{NN}}_{5,\mathbf{q}} = (0,0,-e^{-iq_x},0,1,0),$$

$$\mathbf{B}^{\mathrm{NN}}_{6,\mathbf{q}} = \left(\frac{1}{2}, -\frac{\sqrt{3}}{2}, 0, 0, -\frac{1}{2}e^{-i(-\frac{1}{2}q_x + \frac{\sqrt{3}}{2}q_y)}, \frac{\sqrt{3}}{2}e^{-i(-\frac{1}{2}q_x + \frac{\sqrt{3}}{2}q_y)}\right),$$

and the $\mathbf{B}$ vectors for NNN bonds for each unit cell

$$\mathbf{B}^{\mathrm{NNN}}_{1,\mathbf{q}} = \left(\frac{\sqrt{3}}{2}e^{-iq_x}, \frac{1}{2}e^{-iq_x}, 0, 0, -\frac{\sqrt{3}}{2}, -\frac{1}{2}\right),$$

$$\mathbf{B}^{\mathrm{NNN}}_{2,\mathbf{q}} = (0,0,0,e^{-i(\frac{1}{2}q_x + \frac{\sqrt{3}}{2}q_y)}, 0, -1),$$

$$\mathbf{B}^{\mathrm{NNN}}_{3,\mathbf{q}} = \left(\frac{\sqrt{3}}{2}, \frac{1}{2}, 0, 0, -\frac{\sqrt{3}}{2}e^{-i(\frac{1}{2}q_x + \frac{\sqrt{3}}{2}q_y)}, -\frac{1}{2}e^{-i(\frac{1}{2}q_x + \frac{\sqrt{3}}{2}q_y)}\right),$$

$$\mathbf{B}^{\mathrm{NNN}}_{4,\mathbf{q}} = \left(-\frac{\sqrt{3}}{2}, \frac{1}{2}, \frac{\sqrt{3}}{2}e^{-i(-\frac{1}{2}q_x + \frac{\sqrt{3}}{2}q_y)}, -\frac{1}{2}e^{-i(-\frac{1}{2}q_x + \frac{\sqrt{3}}{2}q_y)}, 0, 0\right), \tag{A9}$$

$$\mathbf{B}^{\mathrm{NNN}}_{5,\mathbf{q}} = (0,0,0,1,0,-e^{-i(-\frac{1}{2}q_x + \frac{\sqrt{3}}{2}q_y)}),$$

$$\mathbf{B}^{\mathrm{NNN}}_{6,\mathbf{q}} = \left(-\frac{\sqrt{3}}{2}e^{iq_x}, \frac{1}{2}e^{iq_x}, \frac{\sqrt{3}}{2}, -\frac{1}{2}, 0, 0\right).$$

## APPENDIX B: CALCULATION OF THE ASYMPTOTIC FOR OF THE $f(\kappa_m,\omega)$ FUNCTION AT SMALL $\kappa_m$

### A. The reduced dynamical matrix

To calculate the asymptotic form of $f(\kappa_m,\omega)$ we first simplify the problem by reducing the dynamical matrix into the space of its three low-energy modes by integrating out its three high-energy modes [15]. The resulting low-energy dynamical matrix is conveniently represented in the basis of longitudinal and transverse phonons and the rotational mode (mode $\nu_3$),

$$(\nu_1', \nu_2', \nu_3') = \left(\frac{q_x\nu_1 + q_y\nu_2}{|\mathbf{q}|}, \frac{-q_y\nu_1 + q_x\nu_2}{|\mathbf{q}|}, \nu_3\right), \tag{B1}$$

in which the dynamical matrix takes the form

$$\tilde{\mathbf{D}}^{(R)} = k\begin{pmatrix} \frac{3q^2}{16} & 0 & \frac{q^2}{16}\cos 3\theta \\ 0 & \frac{q^2}{16} & -\frac{q^2}{16}\sin 3\theta \\ \frac{q^2}{16}\cos 3\theta & -\frac{q^2}{16}\sin 3\theta & \frac{q^2}{16} + \frac{6\kappa_m}{k} \end{pmatrix} \tag{B2}$$

in leading order of small $\kappa$ and quadratic order in $q$ (the cross term of order $\kappa_m q^2$ is considered higher order and has been dropped).

Eigenmodes of the dynamical matrix are identified by diagonalizing $\tilde{\mathbf{D}}^{(R)}$. Strong mixing between the transverse mode and the rotational mode occurs along $q_x = 0$ (i.e., $\theta = 0$) and symmetry equivalent isostatic directions. The resulting two eigenvalues (by diagonalizing the lower right $2 \times 2$ block) are

$$\tilde{\omega}_A^2(q) = \frac{q^2}{16} + 3\kappa_m - \sqrt{\left(\frac{q^2}{16}\right)^2 + (3\kappa_m)^2},$$
$$\tilde{\omega}_B^2(q) = \frac{q^2}{16} + 3\kappa_m + \sqrt{\left(\frac{q^2}{16}\right)^2 + (3\kappa_m)^2}, \tag{B3}$$

obtained from the quadratic order of the renormalized $3 \times 3$ matrix $\tilde{\mathbf{D}}^{(R)}$. The lower eigenvalue $\tilde{\omega}_A^2$corresponds to the *anomalous mode*, which is close to the transverse mode $\nu_2'$ (which is simply $\nu_1$ for $q_x = 0$ direction) for $q_y \ll q_H^* = 4\sqrt{3\kappa_m/k}$ . For $q_y \gg q_H^*$ this anomalous mode corresponds to the linear combination of $(\nu_2' - \nu_3')/2$, which is actually the floppy mode of the kagome lattice in the $\kappa_m \to 0$ limit, in which $\tilde{\omega}_A \to 0$.

### B. Leading order divergence of $f(\kappa_m, \omega)$

The function $f(\kappa_m, \omega)$, as given in Eq. (33), can be analyzed using the simplified dynamical matrix (B2), which is the leading order form in small $\kappa_m$ and $q$. Thus, we can obtain an asymptotic analytical calculation of the integral $f$ by projecting from the six-dimensional basis in Eq. (12) onto the three-dimensional basis in Eq. (B1) built from the three low-energy modes of the system

$$f(\kappa_m, \omega) = -\int_{1\mathrm{BZ}} \frac{d^2\mathbf{q}}{8\pi^2/\sqrt{3}} \mathbf{B}_{1,-\mathbf{q}}^{\mathrm{NNN}} \cdot \mathbf{G}_{\mathbf{q}}(\omega) \cdot \mathbf{B}_{1,\mathbf{q}}^{\mathrm{NNN}}$$
$$\simeq -\int_{1\mathrm{BZ}} \frac{d^2\mathbf{q}}{8\pi^2/\sqrt{3}} \mathbf{B}_{1,-\mathbf{q}}^{\mathrm{NNN}} \cdot \Theta^{\mathrm{T}}\Theta \cdot \mathbf{G}_{\mathbf{q}}(\omega) \cdot \Theta^{\mathrm{T}}\Theta \cdot \mathbf{B}_{1,\mathbf{q}}^{\mathrm{NNN}}, \tag{B4}$$

where

$$\Theta = \begin{pmatrix} \frac{q_x}{\sqrt{3}q} & \frac{q_y}{\sqrt{3}q} & \frac{q_x}{\sqrt{3}q} & \frac{q_y}{\sqrt{3}q} & \frac{q_x}{\sqrt{3}q} & \frac{q_y}{\sqrt{3}q} \\ -\frac{q_y}{\sqrt{3}q} & \frac{q_x}{\sqrt{3}q} & -\frac{q_y}{\sqrt{3}q} & \frac{q_x}{\sqrt{3}q} & -\frac{q_y}{\sqrt{3}q} & \frac{q_x}{\sqrt{3}q} \\ -\frac{1}{\sqrt{3}} & 0 & \frac{1}{2\sqrt{3}} & -\frac{1}{2} & \frac{1}{2\sqrt{3}} & \frac{1}{2} \end{pmatrix} \tag{B5}$$

is the orthogonal transformation from the basis of $\mathbf{u}_\ell = (u_{\ell,1,x}, u_{\ell,1,y}, u_{\ell,2,x}, u_{\ell,2,y}, u_{\ell,3,x}, u_{\ell,3,y})$ to the basis $(\nu_1', \nu_2', \nu_3')$ in Eq. (B1) with the longitudinal, transverse, and rotational modes. In these new bases, the dynamical matrix is modified by integrating out the high-energy modes and keeping to leading order in small $\kappa_m$ and $q$, which lead to the simple form of Eq. (B2) [15], and thus the Green's function can be analyzed correspondingly. Note that we use the Green's function $\tilde{\mathbf{G}}_{\mathbf{q}}(\omega)$ calculated from the renormalized dynamical matrix (B2), so it is different from the bare value $\Theta \cdot \mathbf{G}_{\mathbf{q}}(\omega) \cdot \Theta^{\mathrm{T}}$. The transformed $\mathbf{B}_{1,\mathbf{q}}^{\mathrm{NNN}}$ vector in the basis of $(\nu_1', \nu_2', \nu_3')$ takes the form

$$\left( \frac{(e^{-iq_x} - 1)(3q_x + \sqrt{3}q_y)}{6|\mathbf{q}|}, \frac{(e^{-iq_x} - 1)(\sqrt{3}q_x - 3q_y)}{6|\mathbf{q}|}, -\frac{1}{2}(1 + e^{-iq_x}) \right). \tag{B6}$$

The leading order term of this integral in small $\kappa_m$ is from $\nu_3'$, the anomalous mode, which has a small frequency of order $\sqrt{\kappa_m}$ over the whole range of momentum from $q_H$ to the edge of the Brillouin zone along the isostatic directions, and thus corresponds to diverging contributions to the $f$ integral in small $\kappa_m$.

For an approximation of the $f$ integral at small $\kappa_m$, we use the dynamical matrix of the form (B2), which is kept to leading order in $\kappa_m$ and quadratic order in $q$. At small momentum, the dynamical matrix (B2) is diagonalized by the basis $(\nu_1', \nu_2', \nu_3')$, and the Green's function $\mathbf{G}_{\mathbf{q}}(\omega)$ takes the form of a diagonal matrix

$$\tilde{\mathbf{G}}_{\mathbf{q}}(\omega) = \mathrm{Diag}\left( \frac{1}{\omega^2 - \frac{3q^2}{16}}, \frac{1}{\omega^2 - \frac{q^2}{16}}, \frac{1}{\omega^2 - 6\kappa_m - \frac{q^2}{16}} \right), \tag{B7}$$

which is isotropic and valid for small momentum $|\mathbf{q}| < q_H^*$. Thus, the small momentum region contributes to $f$ the following terms:

$$f_<(\kappa_m, \omega) = -\int_{|\mathbf{q}|<q_H^*} \frac{dq_x dq_y}{8\pi^2/\sqrt{3}} \left\{ \frac{(1 - \cos q_x)(3q_x + \sqrt{3}q_y)^2}{18(q_x^2 + q_y^2)\left(\omega^2 - \frac{3(q_x^2+q_y^2)}{16}\right)} + \frac{(1 - \cos q_x)(\sqrt{3}q_x - 3q_y)^2}{18(q_x^2 + q_y^2)\left(\omega^2 - \frac{q_x^2+q_y^2}{16}\right)} + \frac{1 + \cos q_x}{2\left(\omega^2 - 6\kappa - \frac{q_x^2+q_y^2}{16}\right)} \right\}. \tag{B8}$$

At large momentum, the dynamical matrix can be diagonalized to leading order in $\kappa_m$ in the basis $(\nu_1', \frac{\nu_2'+\nu_3'}{\sqrt{2}}, \frac{\nu_2'-\nu_3'}{\sqrt{2}})$, in which $\mathbf{B}_{1,\mathbf{q}}$ takes the form

$$\left( \frac{(e^{-iq_x} - 1)(3q_x + \sqrt{3}q_y)}{6|\mathbf{q}|}, \frac{(e^{-iq_x} - 1)(\sqrt{3}q_x - 3q_y)}{6\sqrt{2}|\mathbf{q}|} - \frac{1}{2\sqrt{2}}(1 + e^{-iq_x}), \frac{(e^{-iq_x} - 1)(\sqrt{3}q_x - 3q_y)}{6\sqrt{2}|\mathbf{q}|} + \frac{1}{2\sqrt{2}}(1 + e^{-iq_x}) \right), \tag{B9}$$

and the Green's function $\mathbf{G}_{\mathbf{q}}(\omega)$ takes the form of a diagonal matrix

$$\tilde{\mathbf{G}}_{\mathbf{q}}(\omega) = \mathrm{Diag}\left( \frac{1}{\omega^2 - \frac{3(q_x^2+q_y^2)}{16}}, \frac{1}{\omega^2 - 6\kappa_m - \frac{q_x^2+q_y^2}{16}}, \frac{1}{\omega^2 - \frac{1}{Q_M - Q_S}\left[Q_M\omega_S^2 - Q_S\omega_M^2 - q_y(\omega_S^2 - \omega_M^2)\right] - \frac{3q_x^2}{16}} \right), \tag{B10}$$

which is for the direction of $q_x = 0$, and we have used the approximated form (20) of $\omega_A^2$, which represents the dispersion relation of the anomalous mode at large frequency, as depicted in Fig. 4. For this calculation we use the small $\kappa_m$ values $(\omega_S^*)^2 = 3\kappa_m$ and $(\omega_M^*)^2 = 3\kappa_m$.

For the other two directions one should change the third term in Eq. (B10) from $q_x^2$ into the perpendicular direction of the two isostatic directions accordingly. Thus, we need to divide the first Brillouin zone into three parts ($|\theta - \pi/2| < \pi/6$, $|\theta - \pi/6| < \pi/6$, and $|\theta - 5\pi/6| < \pi/6$) and integrate each of them out separately and then calculate the sum. Here we just do the $|\theta - \pi/2| < \pi/6$ part as an example, which uses the form of the Green's function in Eq. (B10). This part of the integral is

$$f_{>,\frac{\pi}{2}}(\kappa_m,\omega) = -\frac{2}{8\pi^2/\sqrt{3}}\int_{q_H^*}^{\frac{2\pi}{\sqrt{3}}} dq_y \int_{-\frac{|q_y|}{\sqrt{3}}}^{\frac{|q_y|}{\sqrt{3}}} dq_x \left\{ \frac{(1-\cos q_x)(3q_x+\sqrt{3}q_y)^2}{18\left(q_x^2+q_y^2\right)\left(\omega^2 - \frac{3\left(q_x^2+q_y^2\right)}{16}\right)} \right.$$
$$\left. + \frac{(2+\cos q_x)q_x^2 + \sqrt{3}(1-\cos q_x)q_xq_y + 3q_y^2}{6\left(q_x^2+q_y^2\right)\left(\omega^2 - 6\kappa_m - \frac{q_x^2+q_y^2}{16}\right)} + \frac{(2+\cos q_x)q_x^2 + \sqrt{3}(1-\cos q_x)q_xq_y + 3q_y^2}{6\left(q_x^2+q_y^2\right)\left(\omega^2 - \frac{Q_M\omega_S^2 - Q_S\omega_M^2 - q_y\left(\omega_S^2-\omega_M^2\right)}{Q_M-Q_S} - \frac{3q_x^2}{16}\right)} \right\}, \quad \text{(B11)}$$

and the integral for the other two directions can be calculated similarly.

The leading order contribution to $f(\kappa_m,\omega)$ in small $\kappa_m$ is from the third term in Eq. (B11), which represents the isostatic mode. We first consider the $\omega = 0$ case, for which the leading order term of $f(\kappa_m,\omega)$ is

$$f_{\frac{\pi}{2},\text{l.o.}}(\kappa_m,0) = \frac{2}{8\pi^2/\sqrt{3}}\int_{q_H^*}^{\frac{2\pi}{\sqrt{3}}} dq_y \int_{-\frac{|q_y|}{\sqrt{3}}}^{\frac{|q_y|}{\sqrt{3}}} dq_x \frac{(2+\cos q_x)q_x^2 + \sqrt{3}(1-\cos q_x)q_xq_y + 3q_y^2}{6\left(q_x^2+q_y^2\right)\left(\frac{Q_M\omega_S^2 - Q_S\omega_M^2 - q_y\left(\omega_S^2-\omega_M^2\right)}{Q_M-Q_S} + \frac{3q_x^2}{16}\right)}$$
$$\simeq \frac{2}{8\pi^2/\sqrt{3}}\int_{q_H^*}^{\frac{2\pi}{\sqrt{3}}} dq_y \frac{(2+\cos q_x)q_x^2 + \sqrt{3}(1-\cos q_x)q_xq_y + 3q_y^2}{6\left(q_x^2+q_y^2\right)} \frac{\pi}{\sqrt{\frac{Q_M\omega_S^2 - Q_S\omega_M^2 - q_y\left(\omega_S^2-\omega_M^2\right)}{Q_M-Q_S}}} \frac{4}{\sqrt{3}}\delta(q_x)$$
$$\simeq \frac{2(1-\sqrt{2/3})}{\sqrt{\kappa_m}}, \quad \text{(B12)}$$

where we took the limit of $\kappa_m \to 0$ and make use of the identity $\lim_{a\to 0}\frac{1}{a^2+x^2} = (\pi/a)\delta(x)$. Adding up the contribution from $\theta = \pi/6$ and $\theta = 5\pi/6$ part we have

$$f_{\text{l.o.}}(\kappa_m,0) \simeq \frac{5(1-\sqrt{2/3})}{\sqrt{\kappa_m}}. \quad \text{(B13)}$$

Other terms in Eqs. (B8) and (B11) contribute higher order terms in small $\kappa_m$, and are discussed in Sec. IV C.

In the case of $\omega > 0$, the leading order term can be calculated in a similar way

$$f_{\frac{\pi}{2},\text{l.o.}}(\kappa_m,0) = -\frac{2}{8\pi^2/\sqrt{3}}\int_{q_H^*}^{\frac{2\pi}{\sqrt{3}}} dq_y \int_{-\frac{|q_y|}{\sqrt{3}}}^{\frac{|q_y|}{\sqrt{3}}} dq_x \frac{(2+\cos q_x)q_x^2 + \sqrt{3}(1-\cos q_x)q_xq_y + 3q_y^2}{6\left(q_x^2+q_y^2\right)\left(\omega^2 - \frac{Q_M\omega_S^2 - Q_S\omega_M^2 - q_y\left(\omega_S^2-\omega_M^2\right)}{Q_M-Q_S} - \frac{3q_x^2}{16}\right)}$$
$$\simeq \frac{2}{8\pi^2/\sqrt{3}}\int_{q_H^*}^{\frac{2\pi}{\sqrt{3}}} dq_y \frac{1}{2} \frac{2\pi i(16/3)}{2(4/\sqrt{3})\sqrt{\omega^2 - \frac{Q_M\omega_S^2 - Q_S\omega_M^2 - q_y\left(\omega_S^2-\omega_M^2\right)}{Q_M-Q_S}}} \simeq \frac{2}{\sqrt{3\kappa_m}}\left(\sqrt{3 - \frac{\omega^2}{\kappa_m}} - \sqrt{2 - \frac{\omega^2}{\kappa_m}}\right). \quad \text{(B14)}$$

The $q_x$ integral can either be evaluated using the $\delta$ function trick by assuming an infinitesimal imaginary part of $\omega(\omega \to \omega + i\delta)$ or by extending the integral limit of $q_x$ to $(-\infty,\infty)$ (because the integrand decays fast when $q_x$ is large) and using contour integral. We also assumed that $|\sqrt{\frac{Q_M\omega_S^2 - Q_S\omega_M^2 - q_y(\omega_S^2-\omega_M^2)}{Q_M-Q_S}} - \omega^2| \ll 1$ to make the simplification

that $\cos q_x \simeq 1$. Adding up the contribution from $\theta = \pi/6$ and $\theta = 5\pi/6$ part we have

$$f_{\text{l.o.}}(\kappa_m,\omega) \simeq \frac{5}{\sqrt{3\kappa_m}}\left(\sqrt{3-\frac{\omega^2}{\kappa_m}}-\sqrt{2-\frac{\omega^2}{\kappa_m}}\right). \quad \text{(B15)}$$

Other terms in Eqs. (B8) and (B11) contribute higher order terms in small $\kappa_m$ and are discussed in Sec. IV C.

### C. Correction at small frequencies

To get the correction to the asymptotic solution of $\kappa_m(\mathcal{P},\omega)$ as in (B15), in particular the small imaginary part rather than zero at small frequency, we calculate the imaginary part of $f$ at small frequencies and solve for the correction to $\kappa_m(\mathcal{P},\omega)$ perturbatively in the CPA equation.

Because we consider small frequencies $\omega^2 < \kappa_m$, the contribution is from the two acoustic modes, which are isotropic, and thus can be calculated as

$$\text{Im}\, f_L \simeq -\frac{2}{8\pi^2/\sqrt{3}}\int_0^{q_H^*} dq \int_0^{2\pi} d\theta q \times \text{Im}\left[\frac{q^2\cos^2\theta(3\cos\theta+\sqrt{3}\sin\theta)^2}{18\left(\omega^2-\frac{3}{16}q^2+i\delta\right)}\right] \simeq \frac{20}{27}\omega^2, \quad \text{(B16)}$$

and

$$\text{Im}\, f_T \simeq -\frac{2}{8\pi^2/\sqrt{3}}\int_0^{q_H^*} dq \int_0^{2\pi} d\theta q \times \text{Im}\left[\frac{q^2\cos^2\theta(\sqrt{3}\cos\theta-3\sin\theta)^2}{18\left(\omega^2-\frac{1}{16}q^2+i\delta\right)}\right] \simeq 4\omega^2. \quad \text{(B17)}$$

Thus we have the correction to Eq. (B15) that is valid for small $\omega$ as

$$f(\kappa_m,\omega) = \frac{5}{\sqrt{3\kappa_m}}\left(\sqrt{3-\frac{\omega^2}{\kappa_m}}-\sqrt{2-\frac{\omega^2}{\kappa_m}}\right)+i\frac{128}{27}\omega^2. \quad \text{(B18)}$$

We then solve the leading order CPA equation in small $\kappa_m$ nonaffine regime perturbatively using this corrected form of $f$ at small $\omega$ and get

$$\kappa_m(\mathcal{P},\omega) = \kappa_m^{(0)} - \frac{256}{135(1-\sqrt{2/3})}\left(\kappa_m^{(0)}\right)^{3/2} i\omega^2, \quad \text{(B19)}$$

where $\kappa_m^{(0)}$ is the zeroth-order solution (42). This correction is very small and cannot be observed in our numerical solutions within precision.


[1] S. Alexander, Phys. Rep. **296**, 65 (1998).
[2] J. C. Maxwell, Philos. Mag. **27**, 294 (1864).
[3] M. F. Thorpe, J. Non-Cryst. Solids **57**, 355 (1983).
[4] S. Feng and P. N. Sen, Phys. Rev. Lett. **52**, 216 (1984).
[5] S. Arbabi and M. Sahimi, Phys. Rev. B **47**, 695 (1993).
[6] J. C. Phillips, J. Non-Cryst. Solids **34**, 153 (1979).
[7] A. V. Tkachenko and T. A. Witten, Phys. Rev. E **60**, 687 (1999).
[8] S. F. Edwards and D. V. Grinev, Phys. Rev. Lett. **82**, 5397 (1999).
[9] D. A. Head, A. J. Levine, and F. C. MacKintosh, Phys. Rev. Lett. **91**, 108102 (2003).
[10] D. A. Head, F. C. MacKintosh, and A. J. Levine, Phys. Rev. E **68**, 025101 (2003).
[11] J. Wilhelm and E. Frey, Phys. Rev. Lett. **91**, 108103 (2003).
[12] A. J. Liu and S. R. Nagel, Nature (London) **396**, 21 (1998).
[13] C. S. O'Hern, S. A. Langer, A. J. Liu, and S. R. Nagel, Phys. Rev. Lett. **88**, 075507 (2002).
[14] C. S. O'Hern, L. E. Silbert, A. J. Liu, and S. R. Nagel, Phys. Rev. E **68**, 011306 (2003).
[15] A. Souslov, A. J. Liu, and T. C. Lubensky, Phys. Rev. Lett. **103**, 205503 (2009).
[16] X. Mao, N. Xu, and T. C. Lubensky, Phys. Rev. Lett. **104**, 085504 (2010).
[17] M. Lax, Rev. Mod. Phys. **23**, 287 (1951).
[18] D. W. Taylor, Phys. Rev. **156**, 1017 (1967).
[19] P. Soven, Phys. Rev. **178**, 1136 (1969).
[20] R. J. Elliott, J. A. Krumhansl, and P. L. Leath, Rev. Mod. Phys. **46**, 465 (1974).
[21] C. R. Calladine, Int. J. Solids Struct. **14**, 161 (1978).
[22] S. Pellegrino and C. R. Calladine, Int. J. Solids Struct. **22**, 409 (1986).
[23] J. C. Phillips and M. F. Thorpe, Solid State Commun. **53**, 699 (1985).
[24] H. He and M. F. Thorpe, Phys. Rev. Lett. **54**, 2107 (1985).
[25] D. J. Jacobs and M. F. Thorpe, Phys. Rev. E **53**, 3682 (1996).
[26] M. F. Thorpe, D. J. Jacobs, M. V. Chubynsky, and J. C. Phillips, J. Non-Cryst. Solids **266-269**, 859 (2000).
[27] M. V. Chubynsky and M. F. Thorpe, Phys. Rev. E **76**, 041135 (2007).
[28] S. Kirkpatrick, Rev. Mod. Phys. **45**, 574 (1973).
[29] D. Stauffer and A. Aharony, *Introduction to Percolation Theory* (Taylor and Francis, London, 1994), 2nd ed.
[30] W. G. Ellenbroek, Z. Zeravcic, W. van Saarloos, and M. van Hecke, Europhys. Lett. **87**, 34004 (2009).
[31] M. Wyart, Europhys. Lett. **89**, 64001 (2010).
[32] D. J. Jacobs and M. F. Thorpe, Phys. Rev. Lett. **75**, 4051 (1995).
[33] S. Feng, M. F. Thorpe, and E. Garboczi, Phys. Rev. B **31**, 276 (1985).
[34] E. J. Garboczi and M. F. Thorpe, Phys. Rev. B **31**, 7276 (1985).
[35] L. M. Schwartz, S. Feng, M. F. Thorpe, and P. N. Sen, Phys. Rev. B **32**, 4607 (1985).
[36] E. J. Garboczi and M. F. Thorpe, Phys. Rev. B **32**, 4513 (1985).
[37] S. Feng, P. N. Sen, B. I. Halperin, and C. J. Lobb, Phys. Rev. B **30**, 5386 (1984).
[38] C. Heussinger and E. Frey, Phys. Rev. Lett. **97**, 105501 (2006).
[39] E. Huisman and T. C. Lubensky (unpublished).
[40] A. J. Liu, S. R. Nagel, W. van Saarloos, and M. Wyart, e-print arXiv:1006.2365.

[41] C. S. O'Hern, L. E. Silbert, A. J. Liu, and S. R. Nagel, Phys. Rev. E **68**, 011306 (2003).
[42] L. E. Silbert, A. J. Liu, and S. R. Nagel, Phys. Rev. Lett. **95**, 098301 (2005).
[43] W. G. Ellenbroek, E. Somfai, M. van Hecke, and W. van Saarloos, Phys. Rev. Lett. **97**, 258001 (2006).
[44] W. G. Ellenbroek, M. van Hecke, and W. van Saarloos, Phys. Rev. E **80**, 061307 (2009).
[45] M. Wyart, S. R. Nagel, and T. A. Witten, Europhys. Lett. **72**, 486 (2005).
[46] M. Wyart, Ann. Phys. (Paris, Fr.) **30**, 1 (2005).
[47] N. Xu, V. Vitelli, M. Wyart, A. J. Liu, and S. R. Nagel, Phys. Rev. Lett. **102**, 038001 (2009).
[48] V. Vitelli, N. Xu, M. Wyart, A. J. Liu, and S. R. Nagel, Phys. Rev. E **81**, 021301 (2010).
[49] A. Souslov, K. Sun, X. Mao, and T. Lubensky (unpublished).